A perturbative analysis of modulated amplitude waves in Bose–Einstein condensates

Mason A. Porter[a)]
School of Mathematics and Center for Nonlinear Science, Georgia Institute of Technology, Atlanta, Georgia 30332

Predrag Cvitanović
School of Physics and Center for Nonlinear Science, Georgia Institute of Technology, Atlanta, Georgia 30332

We apply Lindstedt's method and multiple scale perturbation theory to analyze spatio-temporal structures in nonlinear Schrödinger equations and thereby study the dynamics of quasi-one-dimensional Bose–Einstein condensates with mean-field interactions. We determine the dependence of the amplitude of modulated amplitude waves on their wave number. We also explore the band structure of Bose–Einstein condensates in detail using Hamiltonian perturbation theory and supporting numerical simulations. © *2004 American Institute of Physics.*
[DOI: 10.1063/1.1779991]

Bose–Einstein condensates (BECs) were observed experimentally in 1995 using dilute vapors of sodium and rubidium. The macroscopic behavior of BECs at zero temperature is modeled by the nonlinear Schrödinger equation in the presence of an external potential. This model has proven to be an excellent one for most experiments on BECs. When the external potential is spatially periodic (e.g., due to an optical lattice, which may be created using counter-propagating laser beams), the spectrum of the BEC exhibits a band stucture (spatial resonance structure). This paper utilizes Hamiltonian perturbation theory and supporting numerical simulations to study this structure in detail.

I. INTRODUCTION

At low temperatures, particles in a dilute gas can reside in the same quantum (ground) state, forming a Bose–Einstein condensate.[1–4] This was first observed experimentally in 1995 with vapors of rubidium and sodium.[5,6] In these experiments, atoms were confined in magnetic traps, evaporatively cooled to temperatures on the order of fractions of microkelvins, left to expand by switching off the confining trap, and subsequently imaged with optical methods.[2] A sharp peak in the velocity distribution was observed below a critical temperature, indicating that Bose–Einstein condensation had occurred.

BECs are inhomogeneous, so condensation can be observed in both momentum and coordinate space. The number of condensed atoms N ranges from several thousand to several million. Confining traps are usually approximated well by harmonic potentials. There are two characteristic length scales: the harmonic oscillator length $a_{ho} = \sqrt{\hbar/(m\omega_{ho})}$ [which is on the order of a few microns], where $\omega_{ho} = (\omega_x \omega_y \omega_z)^{1/3}$ is the geometric mean of the trapping frequencies, and the mean healing length $\chi = 1/\sqrt{8\pi|a|\bar{n}}$, where $\bar{n}$ is the mean density and a, the (two-body) s-wave scattering length, is determined by the atomic species of the condensate.[2,4,7,8] Interactions between atoms are repulsive when $a > 0$ and attractive when $a < 0$. For a dilute ideal gas, $a \approx 0$. The length scales in BECs should be contrasted with those in systems like superfluid helium, in which the effects of inhomogeneity occur on a microscopic scale fixed by the interatomic distance.[2]

If considering only two-body, mean-field interactions, a dilute Bose–Einstein gas can be modeled using a cubic nonlinear Schrödinger equation (NLS) with an external potential, which is also known as the Gross–Pitaevskii (GP) equation. BECs are modeled in the quasi-one-dimensional [quasi-(1D)] regime when the transverse dimensions of the condensate are on the order of its healing length and its longitudinal dimension is much larger than its transverse ones.[2,9–11] In the quasi-1D regime, one employs the 1D limit of a 3D mean-field theory rather than a true 1D mean-field theory, which would be appropriate were the transverse dimension on the order of the atomic interaction length or the atomic size.[9–13]

When examining only two-body interactions, the condensate wave function ("order parameter") $\psi(x,t)$ satisfies a cubic NLS

$$i\hbar \psi_t = -[\hbar^2/(2m)]\psi_{xx} + g|\psi|^2\psi + V(x)\psi, \tag{1}$$

where $|\psi|^2$ is the number density, $V(x)$ is an external potential, $g = [4\pi\hbar^2 a/m][1 + \mathcal{O}(\zeta^2)]$, and $\zeta = \sqrt{|\psi|^2|a|^3}$ is the dilute gas parameter.[2,7,8] Because the scattering length a can be adjusted using a magnetic field in the vicinity of a Feshbach resonance,[14] the contribution of the nonlinearity in (1) is tunable.

Potentials $V(x)$ of interest in the context of BECs include harmonic traps, periodic potentials ("standing light waves"), and periodically perturbed harmonic traps. The existence of quasi-1D cylindrical ("cigar-shaped") BECs motivates the study of periodic potentials without a confining

[a)]Electronic mail: mason@math.gatech.edu

trap along the dimension of the periodic lattice.[15] Experimentalists use a weak harmonic trap on top of the periodic lattice to prevent the particles from spilling out. To achieve condensation, the periodic lattice is typically turned on after the trap. If one wishes to include the trap in theoretical analyses, $V(x)$ is modeled by

$$V(x) = V_0 \sin(\kappa(x - x_0)) + V_1 x^2, \tag{2}$$

where κ is the lattice wave number, V_0 is the height of the periodic lattice, and x_0 is the offset of the periodic potential. (Note that these three quantities can all be tuned experimentally.) The periodic term dominates for small x, but the harmonic trap otherwise becomes quickly dominant. When $V_1 \ll V_0$, the potential is dominated by its periodic contribution for many (20 or more) periods.[16–18] (For example, when $V_0/V_1 = 500$, $\kappa = 10$, and $x_0 = 0$, the harmonic component of $V(x)$ essentially does not contribute for 10 periods.) In this work, we usually let $V_1 = 0$ and focus on periodic potentials. Spatially periodic potentials have been employed in experimental studies of BECs[19,20] and have also been studied theoretically.[9–11,17,18,21–25]

When the optical lattice has deep wells (large $|V_0|$), an analytical description of BECs in terms of Wannier wave functions can be obtained in the tight-binding approximation.[26] The Bose–Hubbard Hamiltonian, which is a better description than (1) in the tight-binding approximation, is derived by expanding the field operator in a Wannier basis of localized wave functions at each lattice site. This Hamiltonian has has three contributions: A kinetic energy term yielding contributions from tunnelling between adjacent wells, an energy offset in each lattice site (due, for example, to external confinement), and a potential energy term characterized by atom–atom interactions (that indicates how much energy it takes to put a second atom into a lattice site that already has one atom present). One can use the Bose–Hubbard Hamiltonian to examine transitions between superfluidity and Mott insulation.[27]

In the present paper, we examine in detail the band structure of BECs in shallow periodic lattices using Hamiltonian perturbation theory and supporting numerical simulations.[28] Our methodology, which yields analytical expressions describing the features of BEC resonance bands, exploits the elliptic function solutions of the NLS in the absence of a potential. Note, however, that this paper does *not* explore the chaotic dynamics of BECs.

II. COHERENT STRUCTURES

We consider uniformly propagating coherent structures with the ansatz $\psi(x - vt, t) = R(x - vt) \exp(i[\theta(x - vt) - \mu t])$, where $R \equiv |\psi|$ is the magnitude (amplitude) of the wave function, v is the velocity of the coherent structure, $\theta(x)$ determines its phase, $\vec{v}_0 \propto \nabla \theta$ is the particle velocity, and μ is the chemical potential (which can be termed an angular frequency from a dynamical systems perspective). Considering a coordinate system that travels with speed v (by defining $x' = x - vt$ and relabeling x' as x) yields

$$\psi(x, t) = R(x) \exp(i[\theta(x) - \mu t]). \tag{3}$$

[From a physical perspective, we consider the case $v = 0$, as $V(x') = V(x - vt)$.] When the (temporally periodic) coherent structure (3) is also spatially periodic, it is called a *modulated amplitude wave* (MAW).[29,30] The orbital stability of MAWS for the cubic NLS with elliptic potentials has been studied by Bronski and co-authors.[9–11] To obtain stability information about the sinusoidal potentials we consider, one takes the limit as the elliptic modulus k approaches zero.[31,32]

When $V(x)$ is periodic, the resulting MAWs generalize the Bloch modes that occur in the theory of linear systems with periodic potentials, as one is considering a nonlinear Floquet–Bloch theory rather than a linear one.[15,20,22,33,34] In this paper, we employ phase space methods and perturbation theory to examine MAWs and their concomitant band structure.

The novelty of our work lies in its illumination of BEC band structure through the use of perturbation theory and supporting numerical simulations to examine $2m':1$ spatial subharmonic resonances in BECs in periodic lattices. Such resonances correspond to spatially periodic solutions ψ of period $2m'$ and generalize the "period doubled" states (in $|\psi|^2$) studied by Machholm et al.[35] which pertain to the experiments of Cataliotti et al.[36]

Previous theoretical work in this area has focused on different aspects of BEC band structure, such as loop structure[37–39] and hysteresis.[40] In contrast to the coherent structures we consider, these authors studied band structure using a Bloch wave ansatz. In our notation, they assumed a priori that $R(x) = R(x + 2\pi/\kappa)$ has the same periodicity of the underlying spatial lattice $V(x)$, whereas we have made no such assumption and instead use Hamiltonian perturbation theory to study the dynamical behavior of $R(x)$. Additionally, the analytical components of these works are confined to two-to-three Fourier mode truncations of the Bloch wave dynamics.[37–39]

Inserting (3) into the NLS (1) and equating real and imaginary parts yields

$$\hbar \mu R(x) = -\frac{\hbar^2}{2m} R''(x) + \left[\frac{\hbar^2}{2m} [\theta'(x)]^2 + g R^2(x) \right.$$
$$\left. + V(x) \right] R(x),$$

$$0 = \frac{\hbar^2}{2m} [2\theta'(x)R'(x) + \theta''(x)R(x)], \tag{4}$$

which gives the following two-dimensional system of nonlinear ordinary differential equations:

$$R' = S,$$

$$S' = \frac{c^2}{R^3} - \frac{2m\mu R}{\hbar} + \frac{2mg}{\hbar^2} R^3 + \frac{2m}{\hbar^2} V(x) R. \tag{5}$$

The parameter c is defined via the relation

$$\theta'(x) = \frac{c}{R^2}, \tag{6}$$

and therefore plays the role of "angular momentum," as discussed by Bronski and co-authors.[10] [Equation (6) is a state-
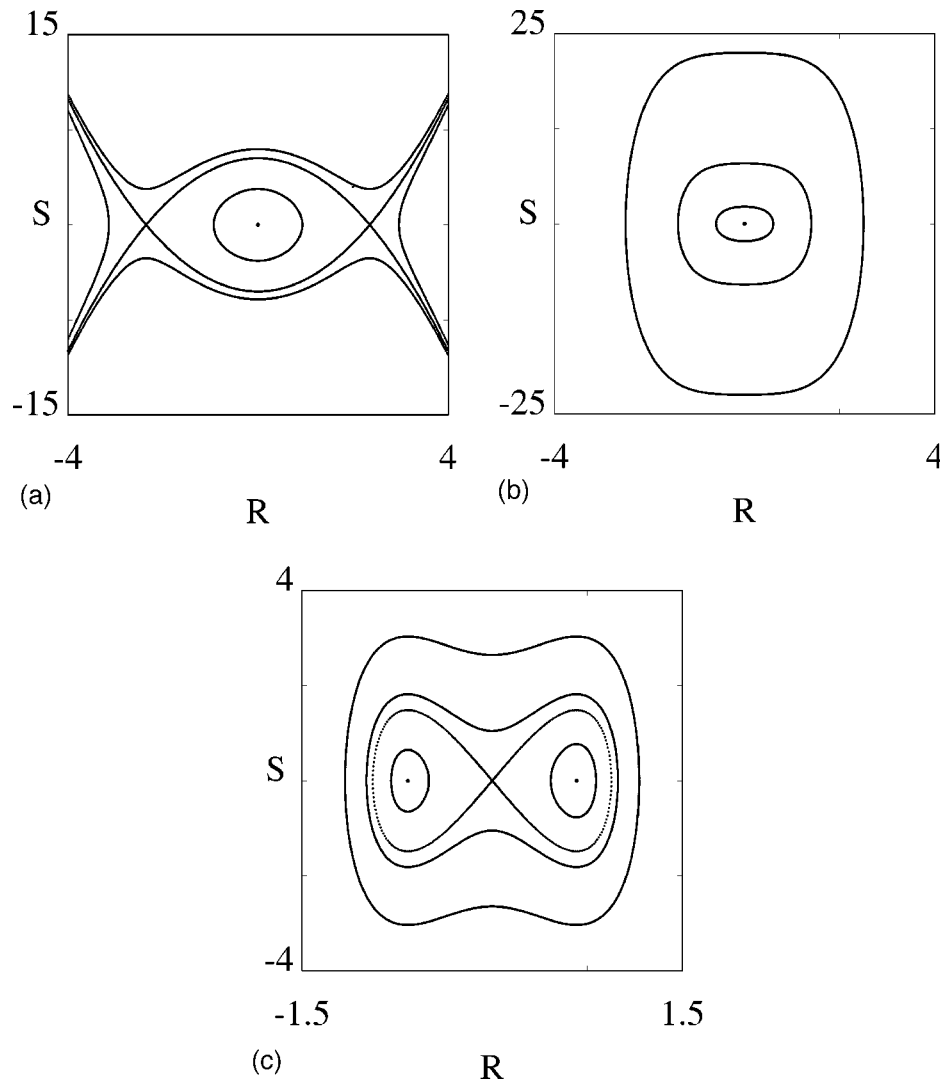
FIG. 1. Phase portraits of coherent structures in BECs with no external potential. The signs of μ and g determine the dynamics of (5). (a) Repulsive BEC with $\mu>0$. The two-body scattering length is $a=0.072$ nm, the value (Ref. 53) for atomic hydrogen (^{1}H). Orbits inside the separatrix (which consists of two heteroclinic orbits) have bounded amplitude $R(x)$. The period of such orbits increases as one approaches the separatrix, whose period is infinite. (b) Attractive BEC with $\mu>0$. The two-body scattering length is $a=-0.9$ nm, the value (Refs. 18 and 54) for ^{85}Rb. (c) Attractive BEC (again ^{85}Rb) with $\mu<0$. Here there are two separatrices, each of which encloses periodic orbits satisfying $R\neq0$.

ment of conservation of angular momentum.] Constant phase solutions, which constitute an important special case, satisfy $c=0$.

III. BECs WITHOUT AN EXTERNAL POTENTIAL

When $V(x)\equiv0$, the dynamical system (5) is autonomous and hence integrable, as it is two-dimensional. Its equilibria (R_*,S_*) satisfy $S_*=0$ and either $R_*=0$, $c=0$ or

$$gR^6-\hbar\mu R^4+\frac{\hbar^2}{2m}c^2=0, \tag{7}$$

which can be solved exactly because it is cubic in R^2. When $c=0$, one obtains $R_*=\pm\sqrt{\hbar\mu/g}$. One thus obtains equilibria at $(R_*,0)\neq(0,0)$ for $g>0$ if $\mu>0$ and $g<0$ if $\mu<0$.

The eigenvalues of the equilibrium $(R_*,0)$ satisfy

$$\lambda^2=-\frac{3c^2}{R_*^4}-\frac{2m\mu}{\hbar}+\frac{6mg}{\hbar^2}R_*^2. \tag{8}$$

When $c=0$ and $R_*=0$, one obtains $\lambda=\pm\sqrt{-2m\mu/\hbar}$. Additionally, one obtains a center at $(0,0)$ when $\mu>0$ and a saddle when $\mu<0$. One also obtains saddles at the $R_*\neq0$ equilibria for $g>0$ when $\mu>0$ and centers at those same locations for $g<0$ when $\mu<0$. These latter equilibria are surrounded by periodic orbits that satisfy $R\neq0$. The possible qualitative dynamics (for $c=0$) are illustrated in Fig. 1 and summarized in Table I.

TABLE I. Type of equilibria of (5) when $V(x)=0$, and $c=0$.

Equilibrium at $(0,0)$	Equilibria at $(R_*,0)\neq(0,0)$	g	μ
Center	None	$-$	$+$
Center	None	0	$+$
Center	Saddles	$+$	$+$
Saddle	None	$+$	$-$
Saddle	None	0	$-$
Saddle	Centers	$-$	$-$

To study the dependence of the wave number of periodic orbits (centered at the origin) of (5) on the amplitude R when $V(x) \equiv 0$, we employ Lindstedt's method[34] and consider null angular-momentum wave functions for the case $\mu > 0$. We also assume $g = \varepsilon \bar{g}$, where $\varepsilon \ll 1$ and $\bar{g} = \mathcal{O}(1)$. The period of $R(x)$ is given by

$$T = \frac{2\pi}{\alpha} = 2\pi \left[1 + \frac{3gA^2}{8\mu\hbar} \right] + \mathcal{O}(\varepsilon^2), \tag{9}$$

where $R(\xi) = R_0(\xi) + \mathcal{O}(\varepsilon)$, $\xi := \alpha x$, $\alpha = 1 + \varepsilon\alpha_1 + \mathcal{O}(\varepsilon^2)$ is the wave number, $A := R_0(0)$, and

$$R_0(\xi) = A \cos\left(\sqrt{\frac{2m\mu}{\hbar}} \xi \right). \tag{10}$$

Note that all periodic orbits are centered at the origin when $\mu > 0$. When $g < 0$, the spatial period becomes smaller with increasing A. When $g > 0$, the period becomes larger with increasing A. In the latter case, the wave number-amplitude relation holds only for solutions inside the separatrix, as the trajectories are unbounded outside the separatrix and hence not periodic.

Before deriving the wave number-amplitude relations when $V(x) \neq 0$, we comment briefly on the preceeding results. The spatial period for small $c \neq 0$ is similar to (9), but it cannot be estimated as easily because Eq. (5) now includes a term of order $\mathcal{O}(R^{-3})$ with coefficient c. Although (9) can be computed exactly in terms of elliptic functions, here we are interested in elucidating the qualitative dynamics of the MAWs of interest as well as establishing the methodology to be employed in the presence of potentials $V(x)$. We will utilize elliptic function solutions in Sec. V in our detailed study of band structure.[28] The physical relevance of elliptic functions to BECs has been discussed by Carr and collaborators.[41,42]

IV. BECs IN A PERIODIC LATTICE

To study the wave number-amplitude relations of periodic orbits in the presence of external potentials, we expand the spatial variable x in multiple scales. We define "stretched space" $\xi := \alpha x$ as in the integrable situation and "slow space" $\eta := \varepsilon x$. We consider potentials of the form $V(x) = \varepsilon \bar{V}(\xi, \eta)$, where $\bar{V}(\xi, \eta) = \bar{V}_0 \sin[\kappa(\xi - \xi_0)] + \bar{V}_1(\eta)$ and $\bar{V}_1$, which is of order $\mathcal{O}(1)$, is arbitrary but slowly varying. Cases of particular interest include $\bar{V}_1 = 0$ (periodic potential) and $\bar{V}_1 = \widetilde{V}_1(\eta - \eta_0)^2$ (superposition of periodic and harmonic potentials).

When $\kappa \neq \pm 2\beta := \pm 2\sqrt{2m\mu/\hbar}$, the equations of motion for the slow dynamics of (5) with $c = 0$ are

$$\frac{dA}{d\eta} \equiv A' = -\beta\alpha_1 B - \frac{3\beta\bar{g}}{8\mu\hbar} BC^2 - \frac{\beta}{2\mu\hbar} B\bar{V}_1(\eta),$$

$$\frac{dB}{d\eta} \equiv B' = \beta\alpha_1 A + \frac{3\beta\bar{g}}{8\mu\hbar} AC^2 + \frac{\beta}{2\mu\hbar} A\bar{V}_1(\eta), \tag{11}$$

where $g \equiv \varepsilon\bar{g}$. The leading-order expression for the amplitude is

$$R_0(\xi, \eta) = A(\eta)\cos(\beta\xi) + B(\eta)\sin(\beta\xi), \tag{12}$$

where $C^2 := A(\eta)^2 + B(\eta)^2$ is a constant. The dynamical system (11) is autonomous when $V_1(\eta) \equiv 0$. Equilibria $(A_*, B_*) \neq (0,0)$ of (11) correspond to periodic orbits of (5) with $c = 0$. The equilibrium value of the squared amplitude is denoted $C_*^2 = A_*^2 + B_*^2$.

Converting to polar coordinates with $A(\eta) = C\cos(\phi(\eta))$ and $B(\eta) = C\sin(\phi(\eta))$ and integrating the resulting equation yields

$$\phi(\eta) = \phi(0) + \left[\alpha_1\beta + \frac{3\beta\bar{g}}{8\mu\hbar} C^2 \right]\eta + \frac{\beta}{2\mu\hbar} \int \bar{V}_1(\eta)d\eta. \tag{13}$$

The wave number of the periodic motion is given by

$$\alpha(C) = 1 - \frac{3g}{8\mu\hbar} C^2 - \frac{1}{2\mu\hbar} V_1(x) + \mathcal{O}(\varepsilon^2). \tag{14}$$

When $\kappa = \pm 2\beta$, we show that the slow flow equations have an extra term due to resonance. Without loss of generality, we let $\kappa = +2\beta$, as changing the sign of V_0 produces the $\kappa = -2\beta$ case. When $m = 0.5$, $\mu = 10$, and $\hbar = 1$, for example, one obtains this resonant situation for $\kappa = \pm 10$. Additionally, we show that C is no longer constant in this resonant situation.

In polar coordinates, the slow flow equations are

$$\phi' = \alpha_1\beta + \frac{3\beta\bar{g}}{8\mu\hbar} C^2 + \frac{\bar{V}_0\beta}{4\mu\hbar} \sin[2(\phi - \beta\xi_0)]$$

$$+ \frac{\beta}{2\mu\hbar} \bar{V}_1(\eta),$$

$$C' = -\frac{\bar{V}_0\beta}{4\mu\hbar} C\cos[2(\phi - 2\beta\xi_0)]. \tag{15}$$

Integrating the equation for C' yields

$$C = C_0 \exp\left[-\frac{\bar{V}_0\beta}{4\mu\hbar} \int \cos[2(\phi(\eta) - \beta\xi_0)]d\eta \right], \tag{16}$$

which one may then insert into the equation for the angular dynamics.

To determine equilibria, one puts $C' = \phi' = 0$. From $C' = 0$, one determines that equilibria (C_*, ϕ_*) satisfy

$$\phi_* = \frac{(2j+1)\pi}{4} + \beta\xi_0, \quad j \in \{0,1,2,3\}, \tag{17}$$

which is independent of the scattering coefficient. Inserting (17) into $C' = 0$ yields the wave number-amplitude relation

$$\alpha_R(C) = \alpha(C) \mp \frac{V_0}{4\mu\hbar} + \mathcal{O}(\varepsilon^2), \tag{18}$$

for periodic orbits of (5). In (18), the minus sign is obtained when $j \in \{0,2\}$, and the plus sign is obtained when $j \in \{1,3\}$. Equation (18) is valid for 2:1 spatial resonances. We examine $2m':1$ resonances for integer m' in Sec. V using Hamiltonian perturbation theory and the elliptic function solutions of (5) when $V_0 = 0$.

To examine the spatial stability (i.e., stability with respect to spatial evolution) of these periodic orbits in the pres-
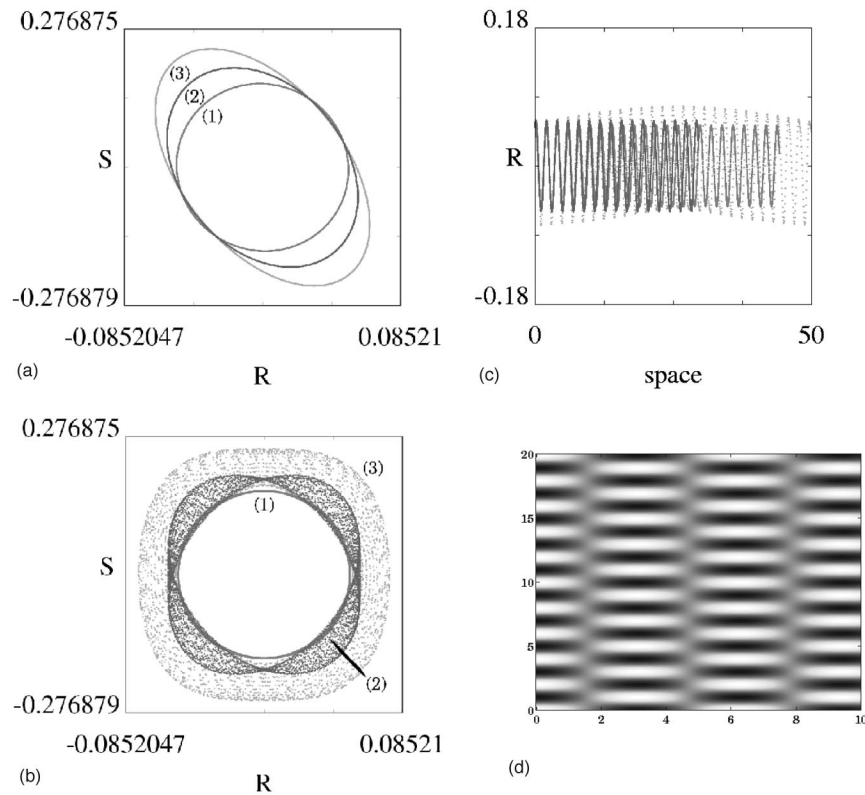
FIG. 2. As the wave number κ of the perturbation is increased, periodic behavior persists for larger $|V_0|$. The initial condition in this plot is $(R(0),S(0))$ $=(0.05,0.05)$, and the parameter values $a=0.072$, $\mu=10$, $m=0.5$, and $x_0=0$ are used for each trajectory. (a) Poincaré section determined by $\sin(\kappa x)=0$. Trajectory (1) corresponds to $(\kappa,V_0)=(100,10)$, trajectory (2) to $(\kappa,V_0)=(100,100)$, and trajectory (3) to $(\kappa,V_0)=(10,10)$. These quasiperiodic solutions indicate the existence of nearby periodic orbits. (b) Phase space plots of the trajectories in (a). Trajectory (1) is the closest to being periodic and trajectory (3) is the furthest away. (c) Amplitude R as a function of space x for trajectories (1)–(3). The band structure of BECs can be studied not only in real space but also in phase space by plotting Poincaré sections and trajectories, as indicated in (a) and (b). Examining the proximity of a trajectory to periodicity is most easily accomplished in phase space. (d) Coherent structure corresponding to quasiperiodic trajectory (1). This plot depicts $Re(\psi)$. The horizontal axis represents time, and the vertical one represents space. The darkest portions are the most negative, and the lightest are the most positive.

ence of resonant periodic potentials, we compute the spatial stability of equilibria of (15) when $V_1(\eta)\equiv0$. The eigenvalues of the periodic orbits are

$$\lambda=\pm\frac{\beta}{2\mu}\sqrt{\mp\frac{3\bar{V}_0\bar{g}C}{2\hbar^2}}.\qquad(19)$$

We show numerical simulations for (5) in the presence of a periodic potential in Fig. 2. In this situation, (5) is a nonlinear Mathieu equation.[32,34,43] Figure 2(d) shows the coherent structure for the trajectory with $\kappa=100$ and $V_0=10$. Figure 3 depicts a Poincaré section describing the dynamics of [85]Rb, for which $a=-0.9$ nm. Figure 4 depicts spatial profiles of the coherent structures corresponding to the locally chaotic and globally chaotic trajectories in Fig. 3.

V. SUBHARMONIC RESONANCES

In this section, we analyze spatial subharmonic resonances and the band structure of repulsive BECs with a positive chemical potential. We perturb off the elliptic function solutions of the underlying integrable system in order to study $2m':1$ spatial resonances with a leading-order perturbation method. Perturbing off simple harmonic functions, by contrast, requires a perturbative method of order m' to study $2m':1$ resonances. At the center of the KAM islands, we

observe "period-multiplied" states. When $m'=1$, one obtains period-doubled states in ψ. As verified numerically in Sec. VI, our qualitative results are excellent. Given that our method is a leading-order one, our quantitative results are also remarkably good.

Recent work by Machholm and co-authors[35] on period-doubled states (in $|\psi|^2$) follows up experimental studies by Cataliotti and co-authors,[36] who observed superfluid current disruption in chains of weakly coupled BECs, which is related to the dependence of the dynamical instability of Bloch states on the magnitude of particle interactions. Period-doubled states, which may be interpreted as soliton trains, arise from dynamical instabilities of the energy bands associated with Bloch states.[35] In the present work, we offer a dynamical systems perspective on period-doubled states and their generalizations. Our theoretical and computational analysis reveals period-multiplied solutions of the GP (1). The existence of these wave functions can be explored experimentally.

A detailed examination of the band structure of BECs in periodic lattices requires a more intricate perturbative analysis than that discussed earlier in this work. Previous authors have concentrated on numerical studies of band structure.[15,22,23] The approach we take, on the other hand, is to analyze the spatial resonance structure that arises from the
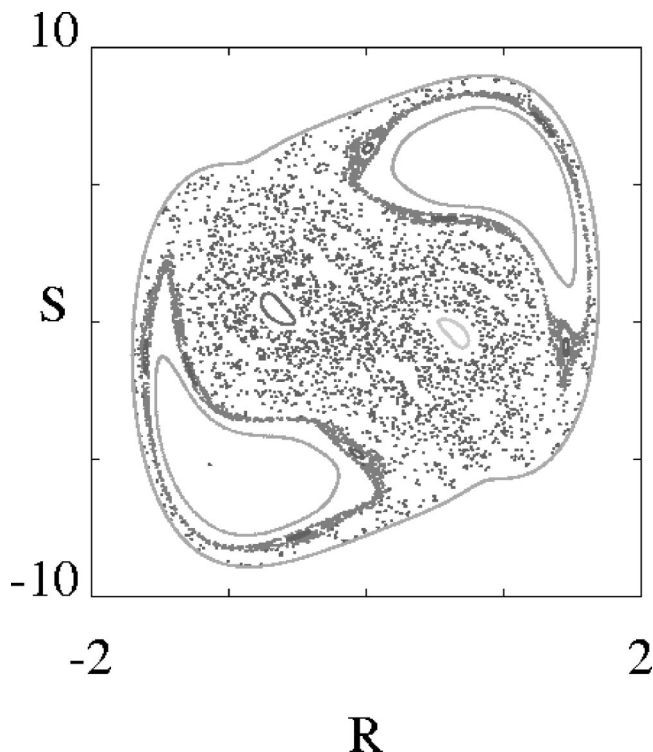
FIG. 3. Poincaré section for the parameter values $\mu = -10$, $m = 0.5$, $x_0 = 0$, $V_0 = 5$, $\kappa = 10$, and $a = -0.9$ nm, corresponding to the experimentally determined scattering length (Refs. 18 and 54) for ^{85}Rb. The depicted trajectories include examples which are quasiperiodic, locally chaotic (near the resonances), and globally chaotic (the stochastic sea).

nonlinear Mathieu equation obtained upon the application of a coherent structure ansatz to the cubic NLS. We examine situations with null angular momentum ($c = 0$), but one observes similar behavior when $c \neq 0$ when R is away from the origin. The analytical approach we employ was introduced by Zounes and Rand[43] for $g < 0$ and $\mu > 0$ [see Fig. 1(b)], the technically easiest case to consider. Their study of nonlinear Mathieu equations is directly applicable to BECs. Our work is an extension of their work to the situation $g > 0$, $\mu > 0$ [see Fig. 1(a)], the second easiest case to consider. We study this case in detail and also apply the results of Zounes and Rand to attractive BECs with a positive chemical potential. We briefly discuss attractive BECs with a negative chemical potential [see Fig. 1(c)], the technically hardest case to consider. Note that this paper does *not* explore the chaotic dynamics of BECs, which is an important open issue.[32,34,44,45]

Let $x_0 = -\pi/(2\kappa)$ and $V_1(x) \equiv 0$ so that

$$V(x) = V_0 \cos(\kappa x). \tag{20}$$

When $c = 0$, the equations of motion (2) and (5) for the amplitude of the coherent structure (3) take the form

$$R'' + \delta R + \alpha R^3 + \epsilon R \cos(\kappa x) = 0, \tag{21}$$

where

$$\delta = \frac{2m\mu}{\hbar}, \quad \alpha = -\frac{2mg}{\hbar^2}, \quad \epsilon = -\frac{2m}{\hbar^2}V_0. \tag{22}$$
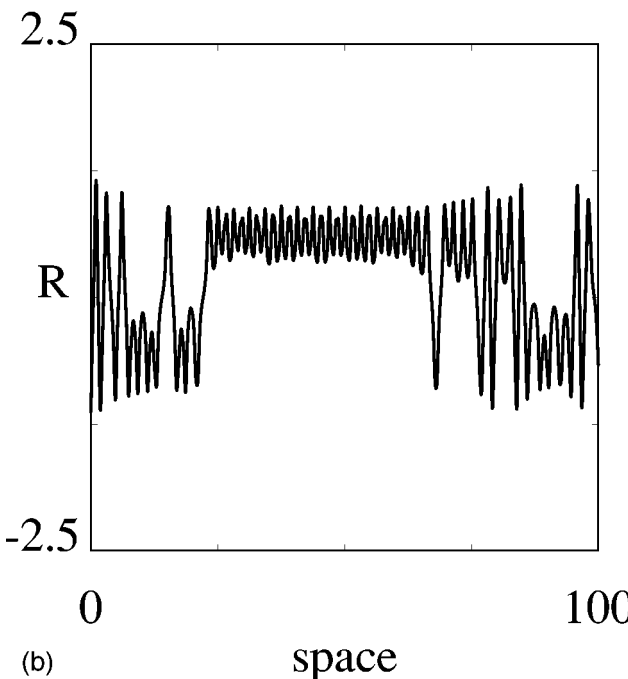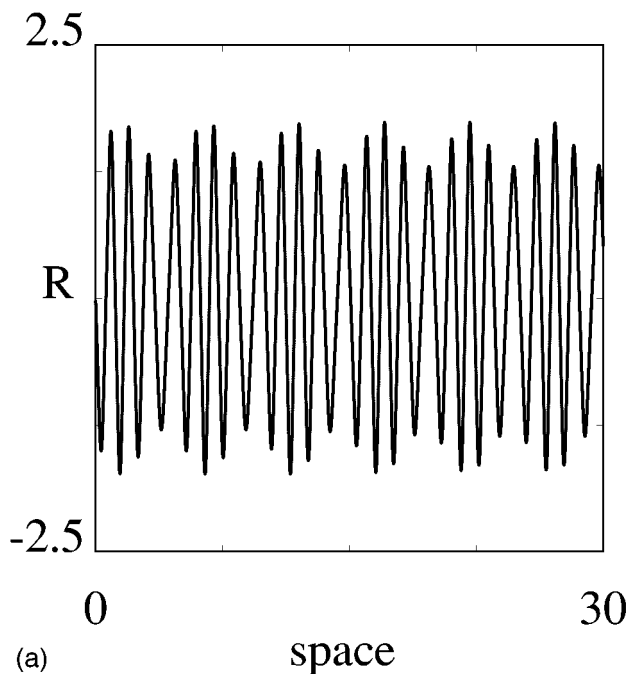

(a)   space

(b)   space

FIG. 4. (a) Spatial profile of the coherent structure corresponding to the locally chaotic trajectory in Fig. 3. The initial conditions are $(R(0), S(0)) \approx (-0.018\,182\,15, -5.232\,683\,58)$. (b) Spatial profile of the coherent structure corresponding to the globally chaotic trajectory in Fig. 3. The initial conditions are $(R(0), S(0)) \approx (-1.132\,835\,30, 1.283\,340\,13)$.

(Note that the perturbation parameter ϵ is not the same as the parameter ε employed earlier.) The parameters μ, V_0, κ, and a (and hence g) can all be adjusted experimentally. When $\epsilon = 0$, solutions of (21) can be written exactly in terms of elliptic functions:[31,32,44,47–49]

$$R = \sigma\rho\,\mathrm{cn}(u, k), \tag{23}$$

where

$$u = u_1 x + u_0, \quad u_1^2 = \delta + \alpha\rho^2,$$

$$k^2 = \frac{\alpha \rho^2}{2(\delta + \alpha \rho^2)}, \tag{24}$$

$$u_1 \geq 0, \quad \rho \geq 0, \quad k^2 \in \mathbb{R}, \quad \sigma \in \{-1, 1\},$$

and u_0 is obtained from an initial condition (and can be set to 0 without loss of generality). We consider $u_1 \in \mathbb{R}$ in order to study periodic solutions. One can use argument transformations to study solutions with complex u_1. When $k^2 \in (1, \infty)$, one makes sense of the cn function with a reciprocal modulus transformation.[46,47] When $k^2 < 0$, one employs a reciprocal complementary modulus transformation, which we discuss below.

Equation (21) can be integrated when $\epsilon = 0$ to yield the Hamiltonian

$$\tfrac{1}{2}R'^2 + \tfrac{1}{2}\delta R^2 + \tfrac{1}{4}\alpha R^4 = h, \tag{25}$$

with given energy h. With (24), one computes

$$h = \frac{1}{4}\rho^2(2\delta + \alpha \rho^2) = \frac{\delta^2}{\alpha} \frac{k^2 k'^2}{(1 - 2k^2)^2}, \tag{26}$$

where $k'^2 := 1 - k^2$. Earlier in this paper, we enumerated the different possibilities for the qualitative dynamics of (21) in terms of the signs of μ and g (and hence in terms of the signs of δ and α).

A. Repulsive BECs with a positive chemical potential

We first consider in detail the case $g > 0$, $\mu > 0$, for which $\delta > 0$, $\alpha < 0$. For notational convenience, we sometimes utilize $\alpha' := -\alpha$. This analysis involves a considerable amount of elliptic-function manipulation, but we are rewarded in the end by a much more effective perturbation theory than can be obtained by employing trigonometric functions.

The center at $(0, 0)$ satisfies $h = \rho^2 = k^2 = 0$. The saddles at $(\pm \sqrt{\delta/\alpha'}, 0)$ and their adjoining separatrix satisfy

$$h = -\frac{\delta^2}{4\alpha}, \quad \rho^2 = \frac{\delta}{|\alpha|}, \quad k^2 = -\infty. \tag{27}$$

The sign $\sigma = +1$ is used for the right saddle, and $\sigma = -1$ is used for the left one. Within the separatrix, all orbits are periodic and the value of σ is immaterial.

1. Action-angle variable description and transformations

For this choice of parameters, $k^2 \in [-\infty, 0]$, so elliptic functions are defined through the reciprocal complementary modulus transformation,[46,47] which relates the (u, k) coordinate system to another coordinate system, which we denote (w, k_2). To transform between these two coordinate systems, one uses the following relations:

$$\begin{aligned} \text{cn}(u, k) &= \text{cd}(w, k_2), \\ \text{dn}(u, k) &= \text{nd}(w, k_2), \\ \text{sn}(u, k) &= k_2' \text{sd}(w, k_2), \end{aligned} \tag{28}$$

$$k' = \frac{1}{k_2'}, \quad u = k_2' w, \quad K = k_2' K_2, \quad E = \frac{1}{k_2'} E_2.$$

Here, $K \equiv K(k)$ denotes the complete elliptic integral of the first kind, $E \equiv E(k)$ denotes the complete elliptic integral of the second kind, and items with the subscript "2" denote the analogous quantities in the (w, k_2) coordinate system.[31,46,48]

We rescale (21) using the coordinate transformation

$$\chi = \sqrt{\delta} x, \quad r = \sqrt{\frac{\delta}{\alpha'}} R, \tag{29}$$

to obtain

$$r'' + r - r^3 = 0, \tag{30}$$

when $V(x) \equiv 0$. (Note that in this analysis, the quantity χ does not represent the mean healing length.) In terms of the original coordinates

$$R(x) = \sqrt{\frac{\delta}{\alpha'}} r(\sqrt{\delta} x) = \sqrt{\frac{\hbar \mu}{g}} r\left(\sqrt{\frac{2m\mu}{\hbar}} x\right). \tag{31}$$

The rescaling applied for other choices of δ and α differ slightly from that in (29), so that the arguments of their associated square roots are positive.

The Hamiltonian corresponding to (30) is

$$H_0(r, s) = \tfrac{1}{2}s^2 + \tfrac{1}{2}r^2 - \tfrac{1}{4}r^4 = h, \quad h \in [0, 1/4], \tag{32}$$

where $s := r' = dr/d\chi$. Additionally, $\rho^2 \in [0, 1]$, $k_2^2 \in [0, 1]$ (corresponding to $k^2 \in (-\infty, 0]$ in the original coordinates), and

$$k^2 = \frac{\rho^2}{2(\rho^2 - 1)}. \tag{33}$$

With the initial condition $r(0) = \rho$, $s(0) = 0$, which implies that $u_0 = 0$, solutions to (30) are given by

$$\begin{aligned} r(\chi) &= \rho \, \text{cn}([1 - \rho^2]^{1/2} \chi, k), \\ s(\chi) &= -\rho[1 - \rho^2]^{1/2} \text{sn}([1 - \rho^2]^{1/2} \chi, k) \\ &\quad \times \text{dn}([1 - \rho^2]^{1/2} \chi, k). \end{aligned} \tag{34}$$

The period of a given periodic orbit Γ is

$$T(k) = \oint_\Gamma d\chi = \frac{4K(k)}{\sqrt{1 - \rho^2}}, \tag{35}$$

where $4K(k)$ is the period in u of $\text{cn}(u, k)$.[48] The frequency of this orbit is

$$\Omega(k) = \frac{\pi \sqrt{1 - \rho^2}}{2K(k)}. \tag{36}$$

Let Γ_h denote the periodic orbit with energy $h = H_0(r, s)$. The area of phase space enclosed by this orbit is constant with respect to χ, so one may define the action[32,46,47,49]

$$J := \frac{1}{2\pi} \oint_{\Gamma_h} s \, dr = \frac{1}{2\pi} \int_0^{T(k)} [s(\chi)]^2 d\chi, \tag{37}$$

which in this case can be evaluated exactly:

$$J = \frac{4\sqrt{1 - \rho^2}}{3\pi} [E(k) - (1 - \rho^2/2)K(k)]. \tag{38}$$

The associated angle[44,45,49,50] in the canonical transformation $(r,s) \rightarrow (J,\Phi)$ is

$$\Phi := \Phi(0) + \Omega(k)\chi. \tag{39}$$

The frequency $\Omega(k)$ monotonically decreases as k^2 goes from $-\infty$ to 0 [that is, as one goes from the separatrix to the center at $(r,s)=(0,0)$]. With this transformation, Eq. (34) becomes

$$r(J,\Phi) = \rho(J)\mathrm{cn}(2K(k)\Phi/\pi,k),$$

$$s(\chi) = -\rho(J)\sqrt{1-\rho(J)^2}\,\mathrm{sn}(2K(k)\Phi/\pi,k)$$
$$\times \mathrm{dn}(2K(k)\Phi/\pi,k), \tag{40}$$

where $k = k(J)$.

After rescaling, the equations of motion for the forced system (21) take the form

$$r'' + r - r^3 + \frac{\epsilon}{\delta}\cos\left(\frac{\kappa}{\sqrt{\delta}}\chi\right)r = 0, \tag{41}$$

with the corresponding Hamiltonian

$$H(r,s,\chi) = H_0(r,s) + \epsilon H_1(r,s,\chi)$$

$$= \frac{1}{2}s^2 + \frac{1}{2}r^2 - \frac{1}{4}r^4 + \frac{\epsilon}{2\delta}r^2\cos\left(\frac{\kappa}{\sqrt{\delta}}\chi\right). \tag{42}$$

In action-angle coordinates, this becomes

$$H(\Phi,J,\chi) = h(J) + \epsilon h_1(\Phi,J,\chi)$$

$$= \frac{1}{2}\rho(J)^2 - \frac{1}{4}\rho(J)^4$$

$$+ \frac{\epsilon}{2\delta}\rho(J)^2\mathrm{cn}^2(2K(k)\Phi/\pi,k)\cos\left(\frac{\kappa}{\sqrt{\delta}}\chi\right). \tag{43}$$

One obtains a second action-angle pair (ϕ,j) using the canonical transformation $(\Phi,J) \rightarrow (\phi,j)$ defined by the relations

$$j(J) = \frac{1}{2}\rho(J)^2, \quad \Phi(\phi,j) = \frac{\phi}{J'(j)}, \tag{44}$$

where

$$k^2 = \frac{j}{2j-1},$$

$$J(j) = \frac{2}{3}\sqrt{1-2j}\,[\tilde{E}(j) - (1-j)\tilde{K}(j)], \tag{45}$$

$$\tilde{K}(j) = \frac{2}{\pi}K[k(j)], \quad \tilde{E}(j) = \frac{2}{\pi}E[k(j)].$$

Additionally,

$$J'(j) := \frac{dJ}{dj} = \sqrt{1-2j}\,\tilde{K}(j) = \frac{1-2j}{\Omega(j)}. \tag{46}$$

Note that $J \sim j$ for small-amplitude motion. Furthermore, $j = 0$ at the origin, and $j = 1/2$ on the separatrix. The Hamiltonian (43) becomes

$$H(\phi,j,\chi) = H_0(j) + \epsilon H_1(\phi,j,\chi)$$

$$= j - j^2 + \frac{\epsilon}{\delta}j\,\mathrm{cn}^2\left(\frac{\tilde{K}(j)}{J'(j)}\phi,k\right)\cos\left(\frac{\kappa}{\sqrt{\delta}}\chi\right). \tag{47}$$

Because we have used elliptic functions rather than trigonometric functions, all results are exact thus far.[43]

2. Perturbative analysis

A subsequent $\mathcal{O}(\epsilon)$ analysis at this stage allows one to study $2m':1$ subharmonic resonances for all $m' \in \mathbb{Z}$. By contrast, had we undertaken this procedure with trigonometric functions (which would have entailed a perturbative approach from the beginning), an $\mathcal{O}(\epsilon^{m'})$ analysis would be required to study $2m':1$ subharmonic resonances of (21).

The Fourier expansion of cn is given by

$$\mathrm{cn}(u,k) = \frac{2\pi}{kK(k)}\sum_{n=0}^{\infty}b_n(k)\cos\left[(2n+1)\frac{\pi u}{2K(k)}\right], \tag{48}$$

where the Fourier coefficients $b_n(k)$ are

$$b_n(k) = \tfrac{1}{2}\mathrm{sech}[(n+1/2)\pi K'(k)/K(k)], \tag{49}$$

and $K'(k) := K(\sqrt{1-k^2})$ denotes the complementary complete elliptic integral of the first kind.[43,48,51] In the present situation

$$\mathrm{cn}\left(\frac{\tilde{K}(j)}{J'(j)}\phi,k\right) = \sum_{n=0}^{\infty}B_n(j)\cos\left[(2n+1)\frac{\phi}{J'(j)}\right], \tag{50}$$

where

$$B_n(j) = \frac{4}{k(j)\tilde{K}(j)}b_n[k(j)]. \tag{51}$$

Consequently,

$$\mathrm{cn}^2\left(\frac{\tilde{K}(j)}{J'(j)}\phi,k\right) = \mathcal{B}_0(j) + \sum_{l=1}^{\infty}\mathcal{B}_l\cos\left(\frac{2l\phi}{J'(j)}\right), \tag{52}$$

where the Fourier coefficients $\mathcal{B}_l(j)$ are obtained by convolving the previous Fourier coefficients (51) with each other.[43]

Before proceeding, it is important to discuss the computation of the coefficients $\mathcal{B}_l(j)$, which require some care. Using the Elliptic Nome[51,52]

$$q(k) := e^{-\pi K'(k)/K(k)}, \tag{53}$$

the Fourier coefficient (49) is expressed as

$$b_n(k) = \frac{1}{q(k)^{n+1/2} + q(k)^{-(n+1/2)}}. \tag{54}$$

One then expands $\mathcal{B}_l(j)$ in Taylor series about $j = 0$. In this computation, one finds that the coefficients of even powers of j in $\mathcal{B}_l(j)$ are the same as when $g < 0$, $\mu > 0$ and that odd powers have the opposite sign. This distinction lies at the root of the qualitatively different dynamics in the two cases, which we will discuss in Sec. V B. Recall that their underlying integrable dynamics are depicted in Fig. 1.

After the Fourier expansion, the perturbative term in the Hamiltonian (47) is

$$H_1(\phi,j,\chi) = \frac{1}{\delta}\mathcal{B}_0(j)\cos\left(\frac{\kappa}{\sqrt{\delta}}\chi\right) + \frac{1}{2\delta}\sum_{l=1}^{\infty}\mathcal{B}_l(j)$$

$$\times\left[\cos\left(\frac{2l\phi}{J'(j)} + \frac{\kappa}{\sqrt{\delta}}\chi\right)\right.$$

$$\left. + \cos\left(\frac{2l\phi}{J'(j)} - \frac{\kappa}{\sqrt{\delta}}\chi\right)\right]. \tag{55}$$

There are infinitely many (subharmonic) resonance bands,[32,44,45] each of which corresponds to a single harmonic in the perturbation series (55). To isolate individual resonances, we apply a canonical, near-identity transformation[32,43–45,49] to the Hamiltonian $H = H_0 + \epsilon H_1$. This transformation is given by

$$\phi = Q + \epsilon\frac{\partial W_1}{\partial P} + \mathcal{O}(\epsilon^2),$$

$$j = P - \epsilon\frac{\partial W_1}{\partial Q} + \mathcal{O}(\epsilon^2), \tag{56}$$

where the generating function W_1 is

$$W_1 = \frac{P\mathcal{B}_0(P)}{\kappa\sqrt{\delta}}\sin\left(\frac{\kappa}{\sqrt{\delta}}\chi\right) + \frac{P}{2\sqrt{\delta}}\sum_{l=1,l\neq m'}^{\infty}\mathcal{B}_l(P)$$

$$\times\left[\frac{\sin\left(\frac{2lQ}{J'(P)} + \frac{\kappa}{\sqrt{\delta}}\chi\right)}{\kappa + 2l\sqrt{\delta}\Omega(P)} + \frac{\sin\left(\frac{2lQ}{J'(P)} - \frac{\kappa}{\sqrt{\delta}}\chi\right)}{\kappa - 2l\sqrt{\delta}\Omega(P)}\right]. \tag{57}$$

To obtain (57), one uses the fact [from (46)] that $\Omega(P) = (1-2P)/J'(P)$.

The resulting Hamiltonian is

$$K(Q,P,\chi) = K_0(P) + \epsilon K_1(Q,P,\chi),$$

$$K_0(P) = P - P^2 = H_0(P), \tag{58}$$

$$K_1(Q,P,\chi) = H_1(Q,P,\chi) + \{H_0,W_1\} - \frac{\partial W_1}{\partial\chi},$$

where $\{A_1,A_2\}$ denotes the Poisson bracket of A_1 and A_2. For the present choice of W_1, one obtains the resonance Hamiltonian

$$K(Q,P,\chi;m') = P - P^2 + \frac{\epsilon}{2\delta}P\mathcal{B}_{m'}(P)\cos\left(\frac{2m'Q}{J'(P)}\right.$$

$$\left. - \frac{\kappa}{\sqrt{\delta}}\chi\right) + \mathcal{O}(\epsilon^2). \tag{59}$$

The choice of the generating function (57) eliminates all resonances from the Hamiltonian K except the $2m':1$ resonance. In focusing on a single resonance band in phase space, one restricts P to a neighborhood of $P_{m'}$, which denotes the location of the m'th resonant torus (associated with periodic orbits in $2m':1$ spatial resonance with the periodic lattice).

3. Resonance relations

Resonant frequencies arise when the denominators of the terms in W_1 vanish,[32,43,44] which yields the equation

$$\frac{\kappa}{\sqrt{\delta}} = \pm 2m'\Omega(P_m), \tag{60}$$

for the resonance of order $2m':1$. As $\Omega \leqslant 1$ is a decreasing function of $P \in [0,1/2)$, the resonance band associated with $2m':1$ subharmonic spatial resonances is present when

$$\frac{\kappa}{\sqrt{\delta}} \leqslant 2m'. \tag{61}$$

For example, when $\kappa = 2.5$ and $\delta = 1$, there are resonances of order 4:1, 6:1, 8:1, etc., but there are no resonances or order 2:1. When $\kappa = 5$ and $\delta = 1$, there are resonances of order 6:1, 8:1, 10:1, etc., but there are no resonances of order 2:1 or 4:1. In terms of the original parameters, the condition (61) describing the onset of $2m':1$ resonance bands takes the form

$$\kappa \leqslant 2m'\sqrt{\frac{2m\mu}{\hbar}}. \tag{62}$$

If the lattice $V(x)$ has a smaller wave number (larger periodicity), then the chemical potential μ has a smaller threshold for a given resonance to occur. As κ is decreased for a fixed μ (i.e., δ) or as μ is increased for a given lattice size κ, resonance bands of lower order emerge from the origin and propagate in phase space. Consequently, a sufficiently high order resonance is always present in (21), but a given number of low-order ones may not be. Lower-order resonances occupy larger regions of phase space, so (61) also indicates the volume of phase space affected by spatial resonances. We will illustrate this in more detail in Sec. VI with numerical simulations.

4. Analytical description of resonance bands

To further examine the resonance structure of (21), we make (59) autonomous via another canonical change of coordinates.[32,43] Toward this end, we define the generating function

$$F(Q,Y,\chi;m') = QY - \frac{\kappa}{2m'\sqrt{\delta}}J(Y)\chi, \tag{63}$$

which yields

$$P = \frac{\partial F}{\partial Q}(Q,Y,\chi) = Y,$$

$$\xi = \frac{\partial F}{\partial Y}(Q,Y,\chi) = Q - \frac{\kappa}{2m'\sqrt{\delta}}J'(Y)\chi$$

$$= Q - \frac{\kappa}{2m'\sqrt{\delta}}J'(P)\chi. \tag{64}$$

(Note that in this analysis, ξ does not represent stretched space, as it did in our multiple scale expansion.) With this final transformation, the resonance Hamiltonian (59) becomes

$$
K_{m'}(\xi,Y) = K(Q,P,\chi;m') + \frac{\partial F}{\partial \chi}(Q,Y,\chi)
$$

$$
= Y - Y^2 - \frac{\kappa}{2m'\sqrt{\delta}}J(Y)
$$

$$
+ \frac{\epsilon}{2\delta}Y\mathcal{B}_{m'}(Y)\cos\left(\frac{2m'\xi}{J'(Y)}\right), \tag{65}
$$

which is integrable in the (Y,ξ) coordinate system. In (R,S)-space, level curves of $K_{m'}$ correspond to invariant curves of Poincaré sections of (21), which are defined by strobing the system when the spatial variable takes the values $x_n = 2n\pi/\kappa$.

We now provide an analytical description of the resonance bands under discussion. In particular, we compute the locations and type of equilibria and width of resonance bands as functions of the parameters δ, ϵ, and κ, and hence of μ, V_0, and κ. Such bands emerge from the action $P=Y=Y_{m'}$, which designates the location of the m'th resonance torus in phase space and is determined by the resonance relation (60):

$$
\frac{\kappa}{\sqrt{\delta}} = 2m'\Omega(Y_{m'}). \tag{66}
$$

This resonance band is associated with periodic orbits in $2m':1$ spatial resonance with the periodic lattice. The resonance torus is filled with degenerate periodic orbits that split[44,45] into $2m'$ saddles and $2m'$ centers when a perturbation is introduced.

From (65), one obtains Hamilton's equations

$$
Y' = -\frac{\partial K_{m'}}{\partial \xi} = \frac{\epsilon Y\mathcal{B}_{m'}(Y)}{J'(Y)}\sin\left(\frac{2m'\xi}{J'(Y)}\right),
$$

$$
\xi' = \frac{\partial K_{m'}}{\partial Y} = 1 - 2Y - \frac{\kappa}{2m'\sqrt{\delta}}J'(Y)
$$

$$
+ \frac{\epsilon}{2\delta}\left[(Y\mathcal{B}_{m'}(Y))'\cos\left(\frac{2m'\xi}{J'(Y)}\right)\right.
$$

$$
\left. + 2m'\xi\frac{J''(Y)}{[J'(Y)]^2}Y\mathcal{B}_{m'}(Y)\sin\left(\frac{2m'\xi}{J'(Y)}\right)\right]. \tag{67}
$$

Equilibria satisfy either $Y=0$ or

$$
\sin\left(\frac{2m'\xi}{J'(Y)}\right) = 0. \tag{68}
$$

They also satisfy

$$
\xi' = 0 = 1 - 2Y - \frac{\kappa}{2m'\sqrt{\delta}}J'(Y) \pm \frac{\epsilon}{2\delta}[Y\mathcal{B}_{m'}(Y)]', \tag{69}
$$

where the sign $\pm$ in (69) arises from

$$
\cos\left(\frac{2m'\xi}{J'(Y)}\right) = 0. \tag{70}
$$

Using $J'(Y) = \sqrt{1-2Y}\widetilde{K}(Y)$, Eq. (69) is written

$$
1 - 2Y - \frac{\kappa}{2m'\sqrt{\delta}}\sqrt{1-2Y}\widetilde{K}(Y) \pm \frac{\epsilon}{2\delta}[Y\mathcal{B}_{m'}(Y)]' = 0. \tag{71}
$$

When $g<0$ and $\mu>0$, the $+$ case yields a saddle and the $-$ case yields a center. In the present situation ($g>0,\mu>0$), this holds for odd m'. When m' is even, $-$ is a saddle and $+$ is a center.

At equilibria, the action Y takes the value

$$
Y_e = Y_{m'} + \epsilon\Delta Y + \mathcal{O}(\epsilon^2) = Y_{m'} \pm \mathcal{O}(\epsilon), \tag{72}
$$

with the signs as in (71). However, note that $Y_c > Y_{m'} > Y_s$, just as for $g<0$. One inserts (72) into (71) and expands the result in a power series. At order $\mathcal{O}(\epsilon^0) = \mathcal{O}(1)$, this reproduces the resonance relation (66). At order $\mathcal{O}(\epsilon)$, one obtains

$$
\Delta Y = \mp \frac{\epsilon}{2\delta}\left[\frac{\mathcal{B}_{m'}(Y_{m'}) + Y_{m'}\mathcal{B}'_{m'}(Y_{m'})}{\Omega(Y_{m'})\sqrt{1-2Y_{m'}}\widetilde{K}'(Y_{m'}) - 1}\right], \tag{73}
$$

where saddles Y_s use the $+$ sign and centers Y_c use the $-$ sign when m' is even, and the opposite is true when m' is odd. When m' is even, $\Delta Y > 0$, but $\Delta Y < 0$ when m' is odd. Additionally, Y_c is always larger than Y_s (for both signs of ϵ).

Resonance bands occupy a finite region of phase space bounded by a pendulum-like separatrix. When a perturbation is introduced, trajectories outside the separatrix behave almost as they would in the absence of a perturbation, so it is important to estimate the width of resonance bands, which emerge at action values satisfying the resonance relation (66). Because of the direction of the inequality in (62), this is more of a condition for nonexistence of given resonances [see the discussion following Eq. (61)]. For a given set of parameters, there will always be resonances of sufficiently high order (i.e., for a sufficiently large m'). However, as we illustrate numerically below, there are parameter regions in which no 2:1 resonances exist, regions in which no 2:1 or 4:1 resonances exist, etc. This behavior contrasts markedly with that observed when $g<0$.[43] In that situation, there exist parameter regions in which only 2:1 resonances exist, regions in which only 2:1 and 4:1 resonances exist, etc.

We now show that the width of a resonance band is

$$
\mathcal{O}\left(\sqrt{\frac{Y_{m'}\mathcal{B}_{m'}(Y_{m'})|\epsilon|}{\delta}}\right), \tag{74}
$$

for perturbations of size $\epsilon = -2mV_0/\hbar^2$.

The separatrix of interest passes through the saddle point Y_s, and the maximum extent of the resonance band occurs at the same phase ξ as the associated center, so

$$
K_{m'}\left(\cos\left(\frac{2m'\xi}{J'(Y_s)}\right) = -1, Y = Y_s\right)
$$

$$
= K_{m'}\left(\cos\left(\frac{2m'\xi}{J'(Y)}\right) = +1, Y\right), \tag{75}
$$

when m' is odd and

$$K_{m'}\left(\cos\left(\frac{2m'\xi}{J'(Y_s)}\right)=+1, Y=Y_s\right)$$

$$=K_{m'}\left(\cos\left(\frac{2m'\xi}{J'(Y)}\right)=-1, Y\right), \tag{76}$$

when m' is even. This implies that

$$(Y-Y_s)-(Y-Y_s)^2-\frac{\kappa}{2m'\sqrt{\delta}}(J(Y)-J(Y_s))$$

$$\pm\frac{\epsilon}{2\delta}(Y\mathcal{B}_{m'}(Y)+Y_s\mathcal{B}_{m'}(Y_s))=0, \tag{77}$$

where the $+$ sign holds for odd m' and the $-$ sign holds for even m'. (Only the $+$ case needs to be considered when $g < 0$ and $\mu > 0$.)

Solutions Y_* of (77) are perturbations to $Y_{m'}$ of the form

$$Y_* = Y_{m'} + W\epsilon^\gamma + \mathcal{O}(\epsilon^{2\gamma}), \tag{78}$$

for an appropriate choice of γ, to be determined by a self-consistency argument. [When $\epsilon < 0$, one writes (78) with $(-\epsilon)^\gamma$ instead. Everything stated here is otherwise the same in that situation.] In this analysis, one uses the fact that $Y_s = Y_{m'} \pm \epsilon(\Delta Y) + \mathcal{O}(\epsilon^2)$, where the $+$ sign is for odd m' and the $-$ sign is for even m'.

To find W and γ, we insert Y_* and Y_s into (77) and expand the resulting expression in a power series about $\epsilon = 0$. During this process, one obtains

$$Y_*^2 = Y_{m'}^2 + 2Y_{m'}W\epsilon^\gamma + W^2\epsilon^{2\gamma},$$

$$J(Y_*) = J(Y_{m'}) + \epsilon^\gamma WJ'(Y_{m'}) + \epsilon^{2\gamma}W^2 J''(Y_{m'})$$

$$+ \mathcal{O}(\epsilon^{3\gamma}), \tag{79}$$

which shows that that the only suitable value of γ is 1/2. Equating terms of order $\mathcal{O}(1)$ yields no new information. Equating terms of order $\mathcal{O}(\epsilon^{1/2})$ yields the resonance relation (66). Equating terms of order $\mathcal{O}(\epsilon)$ shows that

$$W = \left[\pm\frac{Y_{m'}\mathcal{B}_{m'}(Y_{m'})}{\delta\left[1+\frac{\kappa}{2m'\sqrt{\delta}}J''(Y_{m'})\right]}\right]^{1/2}, \tag{80}$$

where the $+$ sign occurs for odd m' and the $-$ sign occurs for even m'. Therefore, the miminal action of the resonance band is

$$Y_{\min} = Y_{m'} - \sqrt{\epsilon}W + \mathcal{O}(\epsilon), \tag{81}$$

and the maximal action is

$$Y_{\max} = Y_{m'} + \sqrt{\epsilon}W + \mathcal{O}(\epsilon). \tag{82}$$

The width of the resonance band is $Y_{\max} - Y_{\min} = 2\sqrt{\epsilon}W + \mathcal{O}(\epsilon)$.

In Sec. VI, we compare these analytical results with numerical simulations.

B. Attractive BECs with a positive chemical potential

Zounes and Rand[43] considered (21) when $\delta > 0$ and $\alpha > 0$ (in other words, $\mu > 0$ and $g < 0$), which is depicted in

TABLE II. Comparison of perturbation theory and numerics for 2:1 resonances ($\kappa = 1.5$, $\delta = 1$). In this table, Y_1 is the action value of the primary resonance, Y_s is the location of its nearby saddle, $(R_s, 0)$ is its location in (R, S)-coordinates, Y_c is the location of the nearby center, $(R_c, 0)$ is its location in (R, S)-space, $Y_{\min}$ is the minimum action value of the separatrix determined from (81), $Y_{\max}$ is the maximum determined from (82), R_{in} is where the inner separatrix crosses the R-axis, R_{out} is where the outer separatrix crosses the R-axis, $Y_{\min,2}$ and $Y_{\max,2}$ are the minimum and maximum actions obtained by solving (77) numerically, and $R_{in,2}$ and $R_{out,2}$ are their corresponding predictions of where the inner and outer separatrices cross the R-axis. The symbol • means a calculation is not applicable and — means it was not computed.

Quantity	$\epsilon = 0.01$		$\epsilon = 0.05$	
	Perturbative	Numerical	Perturbative	Numerical
Y_1	0.281 33	•	0.281 33	•
Y_s	0.279 49	•	0.272 13	•
R_s	± 0.7477	± 0.66	$\pm 0.737\,75$	$\pm(0.56-0.66)$
Y_c	0.283 17	•	0.290 53	•
R_c	± 0.7526	± 0.757	$\pm 0.762\,27$	± 0.774
$Y_{\min}$	0.161 75	•	—	•
$Y_{\max}$	0.400 91	•	—	•
R_{in}	$\pm 0.568\,77$	± 0.66	—	—
R_{out}	$\pm 0.895\,45$	± 0.85	—	—
$Y_{\min,2}$	0.222 03	•	—	•
$Y_{\max,2}$	0.358 07	•	—	•
$R_{in,2}$	$\pm 0.666\,38$	± 0.66	—	—
$R_{out,2}$	$\pm 0.846\,26$	± 0.85	—	—

Fig. 1(b). They did not consider the application of their analysis to Bose–Einstein condensates, so we presently interpret their results in this new light and compare it to our analysis of the repulsive case. When $\delta > 0$, $\alpha > 0$, the phase space of the integrable problem contains no separatrix, and the entire space is foliated by periodic orbits (see Table I). This choice of parameters also leads to the simplest application of the perturbation technique described in Sec. V A. In this case, $k \in [0,1]$, so one need not apply a modulus transformation in the elliptic function solution. One may also set $\sigma = 1$.

We refer the reader to Zounes and Rand[43] for details. Here, we highlight a few results that we wish to contrast directly. When $g < 0$ and $\mu > 0$, the resonance relation one obtains is

$$\frac{\kappa}{\sqrt{\delta}} = 2m'\Omega_a(P_{m'}), \tag{83}$$

where the frequency $\Omega_a(P)$ has a similar form to that of Ω described above. In this situation, $\Omega_a(P) \geq 1$, so subharmonic periodic orbits are present when

$$\frac{\kappa}{\sqrt{\delta}} \geq 2m', \tag{84}$$

which is the reverse inequality as that derived in the repulsive case. Hence, there exist regimes in which *only* 2:1 resonances are present, *only* 2:1 and 4:1 resonances are present, etc. In terms of BEC parameters, the condition (84) describing the onset of $2m'$:1 resonance bands takes the form

TABLE III. Comparison of perturbation theory and numerics for 2:1 resonances ($\kappa=0.75$, $\delta=0.2$). The quantities computed are defined in the caption of Table II.

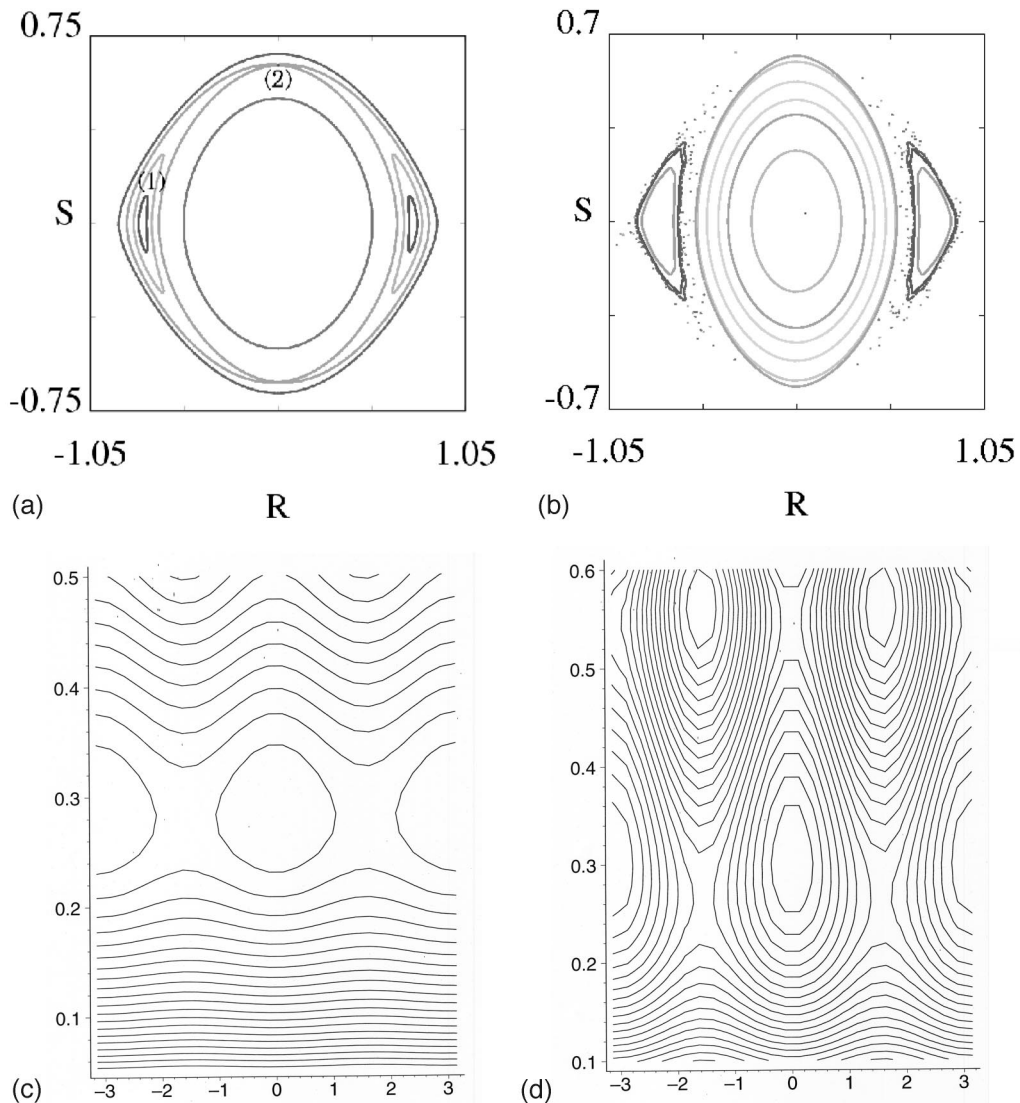| Quantity | $\epsilon=0.01$ | | $\epsilon=0.05$ | |
	Perturbative	Numerical	Perturbative	Numerical
Y_1	0.194 43	•	0.194 43	•
Y_s	0.184 99	•	0.147 18	•
R_s	$\pm272\,02$	$\pm(0.19-0.20)$	$\pm0.242\,64$	—
Y_c	0.203 89	•	0.241 69	•
R_c	$\pm0.285\,58$	±0.2908	$\pm0.310\,93$	±0.335
Y_{min}	0.074 85	•	—	•
Y_{max}	0.314 02	•	—	•
R_{in}	$\pm0.173\,03$	±0.19	—	—
R_{out}	$\pm0.354\,41$	±0.37	—	—
$Y_{min,2}$	0.096 44	•	—	•
$Y_{max,2}$	0.349 04	•	—	•
$R_{in,2}$	$\pm0.196\,40$	±0.19	—	—
$R_{out,2}$	$\pm0.373\,66$	±0.37	—	—

FIG. 5. Poincaré sections (a) and (b) and resonance Hamiltonians K_1 (c) and (d) for $\kappa=1.5$ and $\delta=1$. (a) Poincaré section for $\epsilon=0.01$. The 2:1 resonances are displayed, as indicated by the numbered trajectories. (b) $\epsilon=0.05$. (c) Resonance Hamiltonian for $\epsilon=0.01$ with vertical axis in units of action Y and horizontal axis in units of $\xi/J'(Y)$. (d) Resonance Hamiltonian for $\epsilon=0.05$.

TABLE IV. Comparison of perturbation theory and numerics for 4:1 resonances ($\kappa=2.5$, $\delta=1$). The action value of the secondary resonance is denoted Y_2. Saddles that intersect the R-axis are denoted $(R_s,0)$, and those that intersect the S-axis are denoted $(0,S_s)$. Centers are denoted (R_c,S_c). The other quantities computed are defined in the caption of Table II.

Quantity	$\epsilon=0.01$		$\epsilon=0.05$	
	Perturbative	Numerical	Perturbative	Numerical
Y_2	0.373 58	•	0.373 58	•
Y_s	0.372 94	•	0.370 36	•
R_s	$\pm 0.863\,64$	± 0.88	$\pm 0.860\,65$	± 0.88
S_s	$\pm 0.683\,89$	± 0.687	$\pm 0.682\,93$	± 0.68
Y_c	0.374 22	•	0.376 80	•
(R_c,S_c)	See text	$(\pm 0.691, \pm 0.332)$	See text	$(\pm 0.697, \pm 0.330)$
Y_{min}	0.348 14	•	0.316 70	•
Y_{max}	0.399 02	•	0.430 46	•
$Y_{min,2}$	0.355 71	•	0.329 89	•
$Y_{max,2}$	0.412 37	•	0.462 40	•

$$\kappa \geq 2m' \sqrt{\frac{2m\mu}{\hbar}}. \tag{85}$$

Because the inequalities in (62) and (85) are oppositely directed, adjustments to κ and μ have the opposite effect in these two cases.

Additionally, in this case there is no alternating of signs in the location of saddles and centers in resonance bands, as there is when $g>0$ and $\mu>0$. Because the attractive case with a positive chemical potential is simpler than the one we studied, Zounes and Rand[43] were able to obtain better predictions describing the location of saddles and centers and the width of resonance bands from a perturbation analysis like that discussed in Sec. V A.

C. Attractive BECs with a negative chemical potential

The most difficult case to consider is that of attractive BECs with a negative chemical potential. In (21), $\alpha>0$ and $\delta<0$ (i.e., $\mu<0$), so the integrable dynamics exhibit two homoclinic orbits [see Fig. 1(c)]. The perturbative approach used in this paper must be applied separately inside and outside the separatrix. Orbits inside the separatrix satisfy $h<0$, those on the separatrix satisfy $h=0$, and those outside the separatrix satisfy $h>0$.

Inside the separatrix, $k\in(1,\infty)$, so one must apply the reciprocal modulus transformation to the arguments of the elliptic functions (23) and (24). The sign of σ determines whether one is considering perturbations of periodic orbits in the right half or left half of the phase plane. To utilize our perturbative analysis outside the separatrix, one must expand elliptic functions and elliptic integrals in power series about infinity, where $k=0$. This requires delicate numerical computations of Laurent series coefficients.

In principle, one can overcome the increased technical challenges present in this third case (which is also of interest) and apply the same analysis as in Sec. V A, but the lengthy calculations involved would entail a separate publication.

VI. NUMERICAL SIMULATIONS

To compare the analytical results in Sec. V with numerical simulations, we utilize (R,S) coordinates with $m=1/2$

and $\hbar=1$. To lowest order in ϵ, the change of variables $Y\rightarrow P\rightarrow j$ is a near-identity transformation, so $Y=j+\mathcal{O}(\epsilon)$. Recall from (32) that

$$j=\tfrac{1}{2}\rho^2,$$
$$H_0=h(j)=j-j^2=\tfrac{1}{2}s^2+\tfrac{1}{2}r^2-\tfrac{1}{4}r^4, \tag{86}$$

where $s=\partial r/\partial\chi$. For this comparison, we let $\alpha'=1$ and vary κ, $\delta\equiv\mu$, and $\epsilon\equiv-2mV_0/\hbar^2$. Recall additionally from (29) that

$$r=\sqrt{\frac{g}{\hbar\mu}}R=\sqrt{\frac{\alpha'}{\delta}}R, \quad s=\frac{1}{\mu}\sqrt{\frac{g}{2m}}R'=\frac{\sqrt{\alpha'}}{\delta}R'. \tag{87}$$

A. Methodology

Before discussing our results, we briefly overview our comparison procedure.

The "exact" locations of saddles and centers and sizes of resonance bands were determined using direct numerical simulations of Poincaré sections of (21). The surface of section we employed satisfies $x_n=2n\pi/\kappa$ ($n\in\mathbb{Z}$), which consists of integer multiples of the periodicity of the sinusoidal forcing in (21). In our simulations, the variable κx is periodic, so the surface of section is defined by the condition $\kappa x=0$. We used this framework to find saddles, centers, and resonance band sizes (i.e., separatrix widths) empirically.

To obtain our predictions, we employed the resonance Hamiltonian (65), whose level curves correspond to invariant curves of Poincaré sections. As each trajectory yields a level set of this Hamiltonian, we solved $K'_m=$ constant numerically at appropriate energy values to obtain predictions for the locations of saddles and centers and the size of resonance bands; these latter quantities are determined from the widths of separatrices in (65). For these computations, we expanded elliptic functions and elliptic integrals in Taylor series and subsequently transformed these results to (R,S)-space to compare these calculations with our empirical ones. We also predicted the locations of saddles and centers (72) and (73) and the size of resonances bands (80)–(82) using the predictions obtained from further perturbation expansions. We
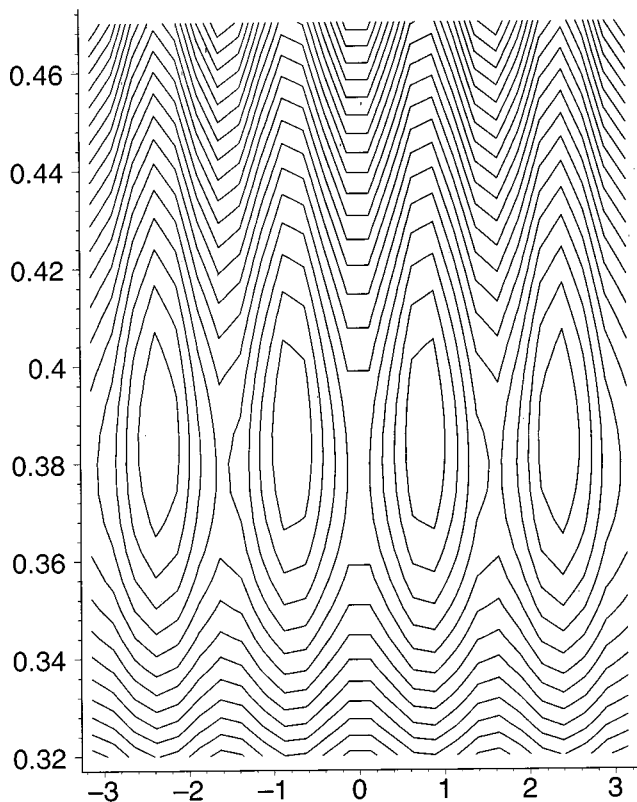
FIG. 6. Resonance Hamiltonian K_2 for $\kappa=2.5$, $\delta=1$, and $\epsilon=0.05$.

again tranformed back to (R,S) space to compare this second set of predictions with our empirical results.
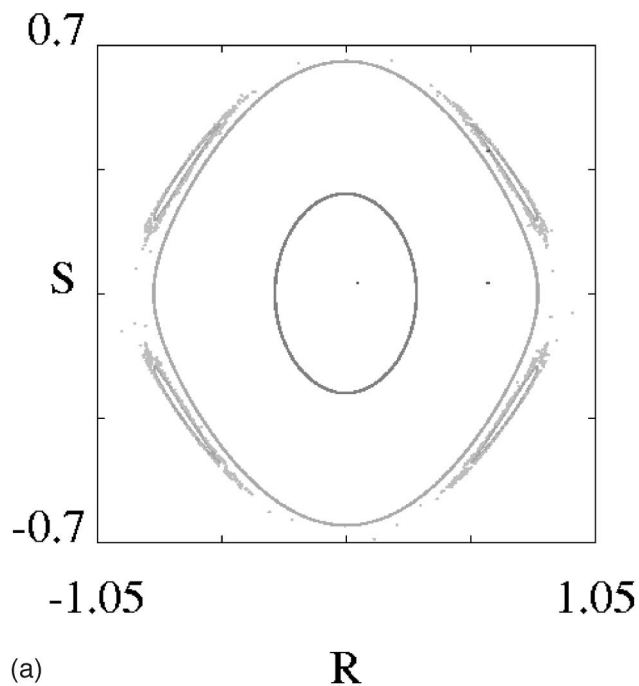
B. Primary resonances

Our comparison between theory and numerics for primary resonances is summarized in Tables II and III.

Consider first $\kappa=1.5$ and $\delta=1$. Poincaré sections and level sets of the resonance Hamiltonian K_1 [in units of $\xi/J'(Y)$] are depicted in Fig. 5. The results of our comparison between perturbation theory and numerical simulations are summarized in Table II.

We do relatively well in locating saddles and extremely well in locating centers. This is especially significant in light of the fact that many canonical transformations were required to obtain our analytical predictions. Although the requisite calculations are complicated, we are rewarded by excellent qualitative agreement and good (and sometimes excellent) quantitative agreement. For $\epsilon=0.05$, the numerical resolution of the location of the saddles was problematic, so a direct comparison is necessarily less accurate. As a result, a range of values is sometimes indicated for the numerically determined location of saddles. Such difficulties with direct numerical simulation emphasize the importance of using qualitative analytical methods to study the features of resonance bands.

Our comparisons between perturbation theory and numerical simulations for $\kappa=0.75$, $\delta=0.2$ are summarized in Table III.

(a)
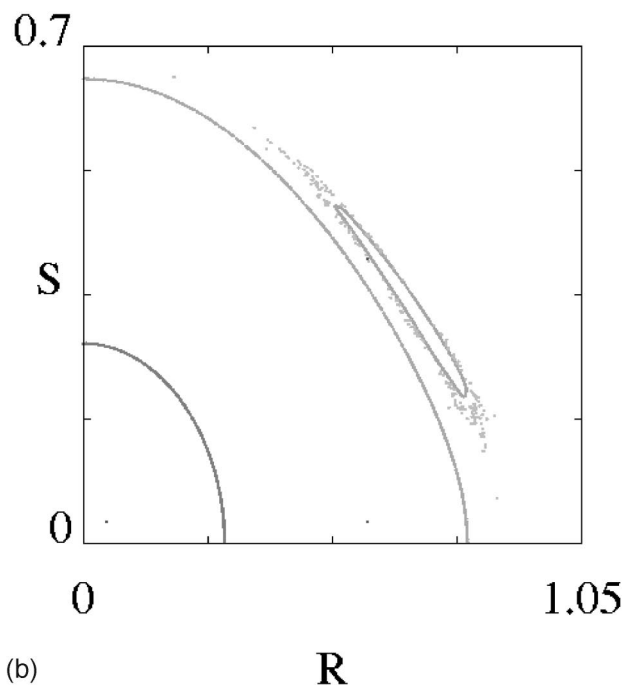
(b)

FIG. 7. (a) Poincaré section for $\kappa=2.5$, $\delta=1$, and $\epsilon=0.05$. Note that there is no 2:1 resonance band for this choice of (κ, δ). The 4:1 resonance is depicted. (b) Upper right corner of (a).

If desired, one can improve these quantitative predictions by including higher-order contributions in the perturbation expansions.

C. Secondary resonances

Our comparison between theory and numerics for secondary resonances is summarized in Table IV.

TABLE V. Comparison of perturbation theory and numerics for 6:1 resonances ($\kappa=3.8$, $\delta=1$, $\epsilon=0.01$). The action value of the tertiary resonance is denoted Y_3. The other quantities computed are defined in the caption of Table II.

Quantity	Perturbative	Numerical
Y_3	0.368 57	•
Y_s	0.368 51	•
R_s	±0.858 50	±(0.859–0.860)
Y_c	0.368 63	•
R_c	±0.858 64	±0.870
Y_{min}	0.362 14	•
Y_{max}	0.375 00	•
$Y_{min,2}$	0.366 14	•
$Y_{max,2}$	0.386 53	•

We study 4:1 resonances for $\kappa=2.5$ and $\delta=1$. No 2:1 resonances exist for this choice of parameters. The resonance Hamiltonian is depicted for $\epsilon=0.05$ in Fig. 6. The corresponding Poincaré section is shown in Fig. 7.

When $\epsilon=0.01$, we observe numerically that centers are located at approximately $(R,S)=(\pm0.691,\pm0.332)$. With $R=\pm0.691$, we predict a value of $S=\pm0.323 84$. With $S=\pm0.332$, we predict a value of $R=\pm0.683 62$. These predictions are remarkably good, as we have used leading-order perturbation theory to derive analytical predictions for 4:1 (secondary) resonances. However, they are not as good as those obtained for the location of saddles in this case or the location of centers for 2:1 (primary) resonances.

When $\epsilon=0.05$, numerical simulations suggest that centers are located at about $(R,S)=(\pm0.697,\pm0.330)$. Using
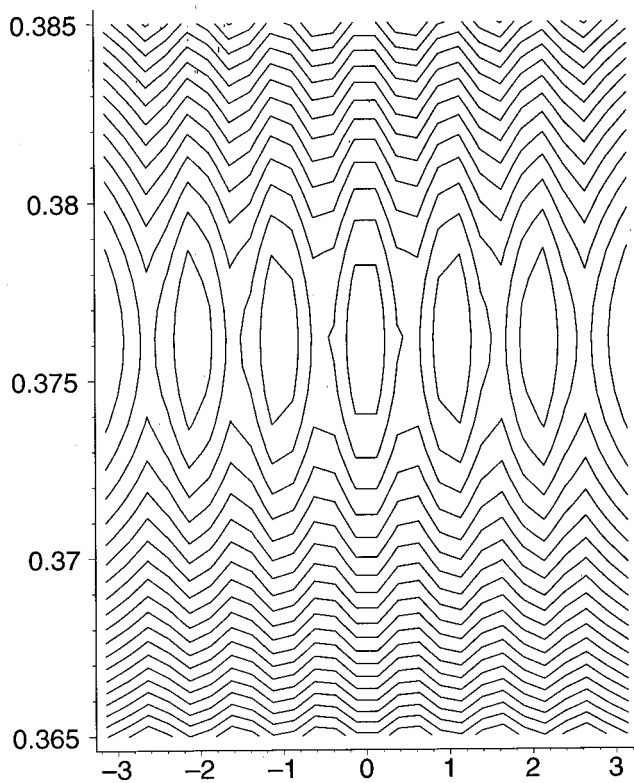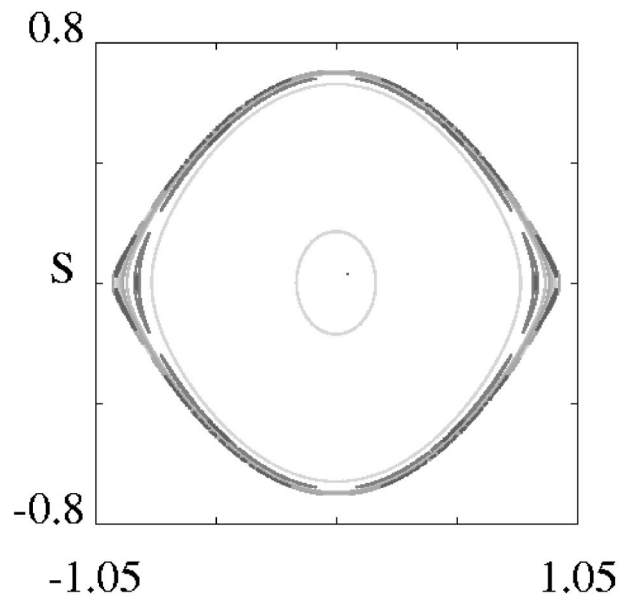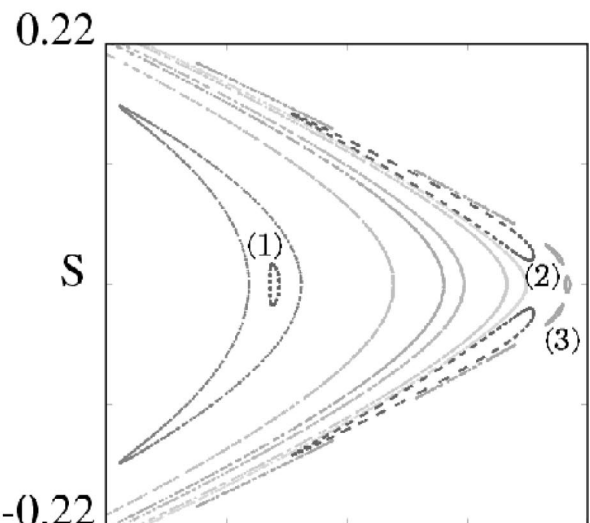

(a)

(b)

FIG. 9. (a) Poincaré section for $\kappa=3.8$, $\delta=1$, and $\epsilon=0.01$. (b) Close-up of the resonances in (a). Both 6:1 (1) and 8:1 (2) resonances are displayed. A higher-order resonance (3) is also depicted. Although not shown, 4:1 resonances are also present for this choice of parameter values.

$R=\pm0.697$ leads to a prediction of $S=\pm0.319 12$. Using $S=\pm0.330$ leads to a prediction of $R=\pm0.687 21$.

D. Tertiary resonances

Our comparison between theory and numerics for tertiary resonances is summarized in Table V.

We consider 6:1 resonances for $\kappa=3.8$, $\delta=1$, and $\epsilon=0.01$. No 2:1 resonances exist for this choice of parameters, but 4:1 resonances do exist. The resonance Hamiltonian is depicted for $\epsilon=0.01$ in Fig. 8. The corresponding

FIG. 8. Resonance Hamiltonian K_3 for $\kappa=3.8$, $\delta=1$, and $\epsilon=0.01$.

Poincaré section is shown in Fig. 9. (The 4:1 resonance bands are not shown in this plot.)

The predictions for centers are not as good as those for saddles, but there is nevertheless good quantitative agreement between observation and prediction, especially considering that a leading-order perturbation method has been employed. Of course, given that higher-order resonances occupy smaller regions of phase space, the absolute errors indicate that these predictions are not as good as the same absolute errors would be when studying lower-order resonances. This caveat notwithstanding, our theoretical analysis does an excellent job of determining the location of resonances and offers a useful tool for locating high-order resonances (and thus studying band structure in great detail) in numerical simulations.

VII. CONCLUSIONS

In this paper, we studied in depth the band structure of BECs in periodic lattices. We approached this problem using a coherent structure ansatz, in contrast to the Bloch wave ansatz of earlier studies.[37,39,41]

Using a technically delicate perturbative approach relying on elliptic function solutions of the integrable NLS, we examined the spatial resonance structure (band structure) of coherent structure solutions of the NLS in considerable detail, providing both an analytical description and numerical verifications of this theory. We derived conditions for the onset of $2m':1$ spatial resonances for all integer m' and developed analytical expressions for the width of these resonance bands and the locations of saddles and centers therein. Comparison with numerical simulations of primary, secondary, and tertiary resonances illustrate the applicability of our analytical theory.

Utilizing a simpler perturbative approach that employs Lindstedt's method and multiple scale analysis, we also established wave number-amplitude relations for coherent structure solutions of the NLS with a periodic potential. In so doing, we explored 2:1 spatial resonances and illustrated the utility of phase space analysis for the study of band structure as well as the structure of modulated amplitude waves in BECs.

In sum, our perturbative approach does an excellent job of determining the location of resonances and analyzing their structure and offers a useful tool for locating high-order resonances (and thus studying BEC band structure in great detail) in numerical simulations. An important open direction, to be addressed in a future publication, is the extent to which the theory developed here is an effective starting point for studies of the chaotic dynamics of BECs.

ACKNOWLEDGMENTS

[1] K. Burnett, M. Edwards, and C. W. Clark, "The theory of Bose–Einstein condensation of dilute gases," Phys. Today 52(12), 37–42 (1999).

[2] F. Dalfovo, S. Giorgini, L. P. Pitaevskii, and S. Stringari, "Theory of Bose–Einstein condensation on trapped gases," Rev. Mod. Phys. 71, 463–512 (1999).

[3] W. Ketterle, "Experimental studies of Bose–Einstein condensates," Phys. Today 52(12), 30–35 (1999).

[4] C. J. Pethick and H. Smith, *Bose–Einstein Condensation in Dilute Gases* (Cambridge University Press, Cambridge, United Kingdom, 2002).

[5] M. H. Anderson, J. R. Ensher, M. R. Matthews, C. E. Wieman, and E. A. Cornell, "Observation of Bose–Einstein condensation in a dilute atomic vapor," Science 269, 198–201 (1995).

[6] K. B. Davis, M.-O. Mewes, M. R. Andrews, N. J. van Druten, D. S. Durfee, D. M. Kurn, and W. Ketterle, "Bose–Einstein condensation in a gas of sodium atoms," Phys. Rev. Lett. 75, 3969–3973 (1995).

[7] B. B. Baizakov, V. V. Konotop, and M. Salerno, "Regular spatial structures in arrays of Bose–Einstein condensates induced by modulational instability," J. Phys. B 35, 5105–5119 (2002).

[8] T. Köhler, "Three-body problem in a dilute Bose–Einstein condensate," Phys. Rev. Lett. 89, 210404 (2002).

[9] J. C. Bronski, L. C. Carr, R. Carretero-González, B. Deconinck, J. N. Kutz, and K. Promislow, "Stability of attractive Bose–Einstein condensates in a periodic potential," Phys. Rev. E 64, 056615 (2001).

[10] J. C. Bronski, L. D. Carr, B. Deconinck, and J. N. Kutz, "Bose–Einstein condensates in standing waves: The cubic nonlinear Schrödinger equation with a periodic potential," Phys. Rev. Lett. 86, 1402–1405 (2001).

[11] J. C. Bronski, L. D. Carr, B. Deconinck, J. N. Kutz, and K. Promislow, "Stability of repulsive Bose–Einstein condensates in a periodic potential," Phys. Rev. E 63, 036612 (2001).

[12] Y. B. Band, I. Towers, and B. A. Malomed, "Unified semiclassical approximation for Bose–Einstein condensates: Application to a BEC in an optical potential," Phys. Rev. A 67, 023602 (2003).

[13] L. Salasnich, A. Parola, and L. Reatto, "Periodic quantum tunnelling and parametric resonance with cigar-shaped Bose–Einstein condensates," J. Phys. B 35, 3205–3216 (2002).

[14] E. A. Donley, N. R. Claussen, S. L. Cornish, J. L. Roberts, E. A. Cornell, and C. E. Weiman, "Dynamics of collapsing and exploding Bose–Einstein condensates," Nature (London) 412, 295–299 (2001).

[15] P. J. Y. Louis, E. A. Ostrovskaya, C. M. Savage, and Y. S. Kivshar, "Bose–Einstein condensates in optical lattices: Band-gap structure and solitons," Phys. Rev. A 67, 013602 (2003).

[16] S. Burger, F. S. Cataliotti, C. Fort, F. Minardi, and M. Inguscio, "Superfluid and dissipative dynamics of a Bose–Einstein condensate in a periodic optical potential," Phys. Rev. Lett. 86, 4447–4450 (2001).

[17] R. Carretero-González and K. Promislow, "Localized breathing oscillations of Bose–Einstein condensates in periodic traps," Phys. Rev. A 66, 033610 (2002).

[18] B. Deconinck, B. A. Frigyik, and J. N. Kutz, "Dynamics and stability of Bose–Einstein condensates: The nonlinear Schrödinger equation with periodic potential," J. Nonlinear Sci. 12, 169–205 (2002).

[19] B. P. Anderson and M. A. Kasevich, "Macroscopic quantum interference from atomic tunnel arrays," Science 282, 1686–1689 (1998).

[20] E. W. Hagley, L. Deng, M. Kozuma, J. Wen, K. Helmerson, S. L. Rolston, and W. D. Phillips, "A well-collimated quasi-continuous atom laser," Science 283, 1706–1709 (1999).

[21] G. L. Alfimov, P. G. Kevrekidis, V. V. Konotop, and M. Salerno, "Wannier functions analysis of the nonlinear Schrödinger equation with a periodic potential," Phys. Rev. E 66, 046608 (2002).

[22] K. Berg-Sørensen and K. Mølmer, "Bose–Einstein condensates in spatially periodic potentials," Phys. Rev. A 58, 1480–1484 (1998).

[23] D.-I. Choi and Q. Niu, "Bose–Einstein condensates in an optical lattice," Phys. Rev. Lett. 82, 2022–2025 (1999).

[24] B. A. Malomed, Z. H. Wang, P. L. Chu, and G. D. Peng, "Multichannel switchable system for spatial solitons," J. Opt. Soc. Am. B 16, 1197–1203 (1999).

[25] A. Trombettoni and A. Smerzi, "Discrete solitons and breathers with dilute Bose–Einstein condensates," Phys. Rev. Lett. 86, 2353–2356 (2001).

[26] C. Menotti, A. Smerzi, and A. Trombettoni, "Superfluid dynamics of a Bose–Einstein condensate in a periodic potential," New J. Phys. 5, 112.1–112.20 (2003).

[27] M. Greiner, O. Mandel, T. Esslinger, T. Hänsch, and I. Bloch, "Quantum phase transition from a superfluid to a Mott insulator in a gas of ultracold atoms," Nature (London) **415**, 39–44 (2002).

[28] M. A. Porter and P. Cvitanović, "Modulated amplitude waves in Bose–Einstein condensates," Phys. Rev. E **69**, 047201 (2004).

[29] L. Brusch, A. Torcini, M. van Hecke, M. G. Zimmermann, and M. Bär, "Modulated amplitude waves and defect formation in the one-dimensional complex Ginzburg–Landau equation," Physica D **160**, 127–148 (2001).

[30] L. Brusch, M. G. Zimmermann, M. van Hecke, M. Bär, and A. Torcini, "Modulated amplitude waves and the transition from phase to defect chaos," Phys. Rev. Lett. **85**, 86–89 (2000).

[31] D. F. Lawden, *Elliptic Functions and Applications*, Number 80 in Applied Mathematical Sciences (Springer-Verlag, New York, 1989).

[32] R. H. Rand, *Topics in Nonlinear Dynamics with Computer Algebra, Volume 1 of Computation in Education: Mathematics, Science and Engineering* (Gordon and Breach, New York, 1994).

[33] N. W. Ashcroft and N. D. Mermin, *Solid State Physics* (Brooks/Cole, Australia, 1976).

[34] R. H. Rand, "Lecture notes on nonlinear vibrations," a free online book available at http://www.tam.cornell.edu/randdocs/nlvibe45.pdf, 2003.

[35] M. Machholm, A. Nicolin, C. J. Pethick, and H. Smith, "Spatial period-doubling in Bose–Einstein condensates in an optical lattice," Phys. Rev. A **69**, 043604 (2004).

[36] F. S. Cataliotti, L. Fallani, F. Ferlaino, C. Fort, P. Maddaloni, and M. Inguscio, "Superfluid current disruption in a chain of weakly coupled Bose–Einstein condensates," New J. Phys. **5**, 71.1–71.7 (2003).

[37] D. Diakonov, L. M. Jensen, C. J. Pethick, and H. Smith, "Loop structure of the lowest Bloch band for a Bose–Einstein condensate," Phys. Rev. A **66**, 013604 (2002).

[38] M. Machholm, C. J. Pethick, and H. Smith, "Band structure, elementary excitations, and stability of a Bose–Einstein condensate in a periodic potential," Phys. Rev. A **67**, 053613 (2003).

[39] B. Wu, R. B. Diener, and Q. Niu, "Bloch waves and Bloch bands of Bose–Einstein condensates in optical lattices," Phys. Rev. A **65**, 025601 (2002).

[40] E. J. Mueller, "Superfluidity and mean-field energy loops; hysteretic behavior in Bose–Einstein condensates," Phys. Rev. A **66**, 063603 (2002).

[41] L. D. Carr, C. W. Clark, and W. P. Reinhardt, "Stationary solutions of the one-dimensional nonlinear Schrödinger equation. I. Case of repulsive non-linearity," Phys. Rev. A **62**, 063610 (2000).

[42] L. D. Carr, Charles W. Clark, and W. P. Reinhardt, "Stationary solutions of the one-dimensional nonlinear Schrödinger equation. II. Case of attractive nonlinearity," Phys. Rev. A **62**, 063611 (2000).

[43] R. S. Zounes and R. H. Rand, "Subharmonic resonance in the non-linear Mathieu equation," Int. J. Non-Linear Mech. **37**, 43–73 (2002).

[44] J. Guckenheimer and P. Holmes, *Nonlinear Oscillations, Dynamical Systems, and Bifurcations of Vector Fields*, Number 42 in Applied Mathematical Sciences (Springer-Verlag, New York, 1983).

[45] S. Wiggins, *Introduction to Applied Nonlinear Dynamical Systems and Chaos*. Number 2 in Texts in Applied Mathematics (Springer-Verlag, New York, 1990).

[46] V. T. Coppola, "Averaging of strongly nonlinear oscillators using elliptic functions," Ph.D. thesis, Cornell University, August 1989.

[47] V. T. Coppola and R. H. Rand, "Chaos in a system with a periodically disappearing separatrix," Nonlinear Dyn. **1**, 401–420 (1990).

[48] E. T. Whittaker and G. N. Watson, *A Course of Modern Analysis*, 4th ed. (Cambridge University Press, Cambridge, Great Britain, 1927).

[49] H. Goldstein, *Classical Mechanics*, 2nd ed. (Addison-Wesley, Reading, MA, 1980).

[50] A. J. Lichtenberg and M. A. Lieberman, *Regular and Chaotic Dynamics*, 2nd ed. Number 38 in Applied Mathematical Sciences (Springer-Verlag, New York, 1992).

[51] *Handbook of Mathematical Functions with Formulas, Graphs, and Mathematical Tables*, edited by M. Abramowitz and I. Stegun, Number 55 in Applied Mathematics Series (National Bureau of Standards, Washington, D.C., 1964).

[52] *Standard Mathematical Tables and Formulae*, edited by D. Zwillinger, 30th ed. (CRC, Boca Raton, FL, 1996).

[53] D. G. Fried, T. C. Killian, L. Willmann, D. Landhuis, S. C. Moss, D. Kleppner, and T. J. Greytak, "Bose–Einstein condensation of atomic hydrogen," Phys. Rev. Lett. **81**, 3811–3814 (1998).

[54] J. L. Roberts, N. R. Claussen, S. L. Cornish, E. A. Donley, E. A. Cornell, and C. E. Wieman, "Controlled collapse of a Bose–Einstein condensate," Phys. Rev. Lett. **86**, 4211–4214 (2001).